

The ionization properties of extreme nearby star-forming regions

Jacopo Chevallard¹*†, Stéphane Charlot², Peter Senchyna³, Daniel P. Stark³,
Alba Vidal-García², Anna Feltre⁴, Julia Gutkin², Tucker Jones^{5,6}‡, Ramesh Mainali³,
Aida Wofford⁷

¹Scientific Support Office, Directorate of Science and Robotic Exploration, ESA/ESTEC, Keplerlaan 1, 2201 AZ Noordwijk, The Netherlands

²Sorbonne Universités, UPMC-CNRS, UMR7095, Institut d’Astrophysique de Paris, F-75014, Paris, France

³Steward Observatory, University of Arizona, 933 N Cherry Ave, Tucson, AZ 85721 USA

⁴Centre de Recherche Astrophysique de Lyon, Université Lyon 1, 9 Avenue Charles André, F-69561 Saint Genis Laval Cedex, France

⁵Department of Physics, University of California Davis, 1 Shields Avenue, Davis, CA 95616, USA

⁶Institute for Astronomy, University of Hawaii, 2680 Woodlawn Drive, Honolulu, HI 96822, USA

⁷Instituto de Astronomía, UNAM, Ensenada, CP 22860, Baja California, Mexico

Accepted . Received ; in original form

ABSTRACT

The bulk of hydrogen-ionizing photons necessary to reionize the intergalactic medium (IGM) by redshift $z \sim 6$ is likely to have arisen from stars in low-mass galaxies. Whether these galaxies were numerous enough at $z > 6$ to reionize the IGM entirely depends on their production rate of H-ionizing photons, ξ_{ion}^* , and the fraction of these escaping into the IGM. We derive a novel diagnostic of ξ_{ion}^* based on the equivalent width of the bright [O III] $\lambda\lambda 4959, 5007$ line doublet, which does not require measurements of H-recombination lines. We calibrate this diagnostic through the analysis of the luminosities of 15 nebular emission lines in high-quality optical spectra of 10 low-redshift analogs of primeval galaxies, using the new-generation spectral analysis tool BEAGLE. The success of this analysis confirms the ability of the models to constrain the ionized-gas properties of extreme star-forming regions, paving the way to similar analyses at high redshift. The new ξ_{ion}^* diagnostic can be used to derive more accurate estimates of this parameter than currently possible from the contamination by $\text{H}\beta + [\text{O III}] \lambda\lambda 4959, 5007$ of broad-band photometry in distant galaxies, and, in the future, from direct observations of [O III] $\lambda\lambda 4959, 5007$ out to $z \sim 9.5$ using *JWST*/NIRSpec.

Key words: galaxies: evolution – galaxies: ISM – galaxies: dwarf – HII regions – dark ages, reionization, first stars – methods: data analysis

1 INTRODUCTION

The appearance of the first stars and galaxies in the Universe at the end of the Dark Ages marked the beginning of the epoch of reionization (EoR, e.g. Bromm & Yoshida 2011). The EoR appears to have lasted mostly between $z \sim 15$ (Planck Collaboration et al. 2016) and $z \sim 6$ (e.g. Fan et al. 2006). Reionization is generally thought to have been mainly driven by young stars in low-mass galaxies (see review by Stark 2016), with minor contributions by active galactic nuclei (e.g. Parsa et al. 2017), X-ray binaries (e.g. Mirabel et al. 2011) and Population-III stars (e.g. Wise et al. 2014). This is supported by the observed steepening of the faint-end slope of the ultraviolet (UV) galaxy luminosity function toward high redshift (e.g. Bouwens

et al. 2015), although the contribution by star-forming galaxies to cosmic reionization depends on several other largely unconstrained quantities. These include the minimum absolute UV magnitude of low-mass galaxies, production rate of H-ionizing photons (\dot{N}_{ion}), fraction of these escaping into the IGM (f_{esc}), and spatial variations of density and temperature in the IGM.

Rough constraints have been set on the rate of H-ionizing photons per unit intrinsic monochromatic UV (1500 Å) luminosity, $\xi_{\text{ion}}^* = \dot{N}_{\text{ion}}/L_{\text{UV}}^*$, from direct (Schaerer et al. 2016, at $z \sim 0.3$) and indirect (i.e., photometric; Bouwens et al. 2016, at $z > 4$) measurements of H-Balmer-line and UV luminosities. These are compatible with canonical predictions of stellar population synthesis models, $\log \xi_{\text{ion}}^* \sim 25.2\text{--}25.3 \text{ erg}^{-1} \text{ Hz}$, although the bluest galaxies observed by Bouwens et al. (2016) and another direct measurement from high-ionization UV lines in a lensed $z \approx 7$ galaxy (Stark et al. 2015b) suggest higher ξ_{ion}^* values in pristine, actively star-forming galaxies, with potentially important implications for reionization.

* E-mail: jchevall@cosmos.esa.int

† ESA Research Fellow

‡ Hubble Fellow

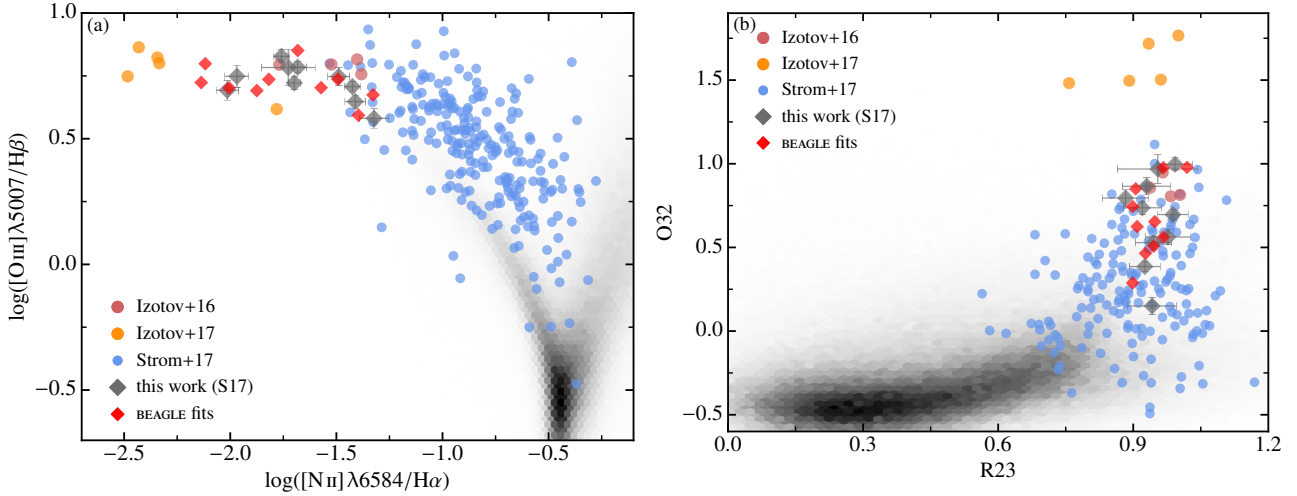


Figure 1. (a) $[\text{N II}]$ BPT diagram showing star-forming galaxies at $z \sim 2-2.6$ from the KBSS survey (blue circles, Strom et al. 2017), the 4 LyC continuum ‘leaker’ at $z \sim 0.3$ from Izotov et al. (2016) (red circles), the 5 compact star-forming galaxies at $z < 0.07$, candidates LyC continuum leakers, from Izotov et al. (2017), and the 10 galaxies presented in S17 analyzed in this work (grey diamonds), along with the model predictions obtained with BEAGLE (red diamonds). As a reference, we also show with a grey-scale (linear) density plot galaxies from the MPA/JHU emission line catalogue based on SDSS DR7 data. MPA/JHU fluxes are corrected for Galactic extinction only, while the other fluxes for internal extinction as well. (b) same as (a), but showing the $\text{O32} = \log([\text{O III}]\lambda\lambda 4959, 5007/[\text{O II}]\lambda\lambda 3726, 3729)$ vs $\text{R23} = \log([\text{O III}]\lambda\lambda 4959, 5007 + [\text{O II}]\lambda\lambda 3726, 3729)/\text{H}\beta$ diagram.

In this Letter, we use the new-generation spectral analysis tool BEAGLE (Chevallard & Charlot 2016) to investigate the ionization properties of 10 extreme nearby star-forming regions found by Senchyna et al. (2017, hereafter S17) to have UV spectra similar to those of $z \sim 6-7$ star-forming galaxies. Our simultaneous fits of 15 emission lines in high-quality optical spectra of these galaxies provide valuable constraints on the properties of the ionizing stars, photoionized gas and attenuation by dust. Beyond the demonstration that the stellar population and photoionization models incorporated into BEAGLE offer accurate fits to the data, this analysis allows us to uncover and calibrate a relation between ξ_{ion}^* and equivalent width (EW) of $(\text{H}\beta + [\text{O III}]\lambda\lambda 4959, 5007)$. This relation extends from canonical ξ_{ion}^* values at low line EW up to nearly an order or magnitude larger for the most extreme galaxies.

2 PHYSICAL PROPERTIES OF IONIZED GAS AND IONIZATION SOURCES

We appeal to a sample of 10 nearby analogs of primeval galaxies, for which our team has acquired high-quality UV data from *HST*/COS (G160M and G185M gratings) and optical spectra from MMT (see S17 for details). These galaxies were selected from a sample of $\text{He II}\lambda 4686$ emitters dominated by stellar photoionization, identified by Shirazi & Brinchmann (2012) from the SDSS DR7 (Abazajian et al. 2009). The galaxies have hard ionizing spectra able to doubly ionize He, i.e. with substantial flux at $\lambda < 228 \text{ \AA}$ (54.4 eV), although only half show Wolf-Rayet (WR) spectral features. Our follow-up *HST* observations of these objects succeeded in revealing high-ionization UV lines ($\text{C IV}\lambda\lambda 1548, 1551$, $\text{C III}\lambda\lambda 1907, 1909$, $\text{O III}\lambda\lambda 1660, 1666$) similar to those typically observed in galaxies at $z \gtrsim 5$ (Stark et al. 2015a,b, 2017; Mainali et al. 2017; Schmidt et al. 2017; Smit et al. 2017), providing a unique reference sample for high-redshift studies.

The location of our galaxies in the ‘ $[\text{N II}]$ ’ Baldwin et al. (1981, BPT) diagram shown in Fig. 1a is typical of sub-solar metallicity gas ($Z/Z_{\odot} \sim 0.1-0.7$) with a high ionization parameter (see, e.g.,

fig. 2 of Gutkin et al. 2016), while the large O32 values at fixed R23, shown in Fig. 1b, indicate a hard ionizing spectrum. Fig. 1a also shows that our galaxies have lower $[\text{N II}]\lambda 6584/\text{H}\alpha$, at fixed $[\text{O III}]\lambda 4959/\text{H}\beta$, than those in the KBSS sample of Strom et al. (2017). These ratios are similar to those of the $z \sim 0.3$ LyC leakers of Izotov et al. (2016), although they do not reach the extreme $[\text{N II}]\lambda 6584/\text{H}\alpha \sim -2.5$ of the compact star-forming galaxies of Izotov et al. (2017). Interestingly, Fig. 1b shows no significant offset between our galaxies, the KBSS sample and the LyC leakers in the O32 vs R23 diagram, while Izotov et al. (2017) specifically targeted extreme O32 emitters. We also note the presence of a broad (a few $\times 10^2$ km/s) component in several emission lines ($[\text{O III}]\lambda\lambda 4959, 5007$, $\text{H}\beta$, $\text{H}\alpha$), at a level of a few per cent the intensity of the narrow component. Such broad components have been observed in other low-mass, low-metallicity, highly star-forming galaxies and linked to energy injection from stellar winds and supernovae (e.g. Izotov et al. 2007; James et al. 2009; Amorín et al. 2012). We defer a more detailed discussion to a future paper.

2.1 Stellar-population and photoionization modelling

We derive the ionized-gas properties of the galaxies in our sample by considering a set of 15 optical emission lines from SDSS and MMT observations: 4 H-Balmer lines ($\text{H}\alpha$, $\text{H}\beta$, $\text{H}\gamma$, $\text{H}\delta$), 4 oxygen lines/line doublet ($[\text{O II}]\lambda\lambda 3726, 3729$, $[\text{O III}]\lambda 4363$, $[\text{O III}]\lambda 4959$, $[\text{O III}]\lambda 5007$), each component of the nitrogen ($[\text{N II}]\lambda 6548$, $[\text{N II}]\lambda 6584$) and sulfur ($[\text{S II}]\lambda 6716$, $[\text{S II}]\lambda 6731$) doublets, and $[\text{Ne III}]\lambda 3868$, $\text{He I}\lambda 5875$ and $[\text{Ar III}]\lambda 7135$. We correct the observed line fluxes for Galactic extinction as outlined in section 2.7 of S17 and fit them with BEAGLE after rescaling the errors on SDSS fluxes by a factor 1.8, the average error correction suggested by the MPA/JHU analysis.¹ BEAGLE incorporates the self-consistent treatment of the emission from stars (we use the latest version of the Bruzual & Charlot 2003 stellar population synthesis code) and

¹ https://wwwmpa.mpa-garching.mpg.de/SDSS/DR7/raw_data.html

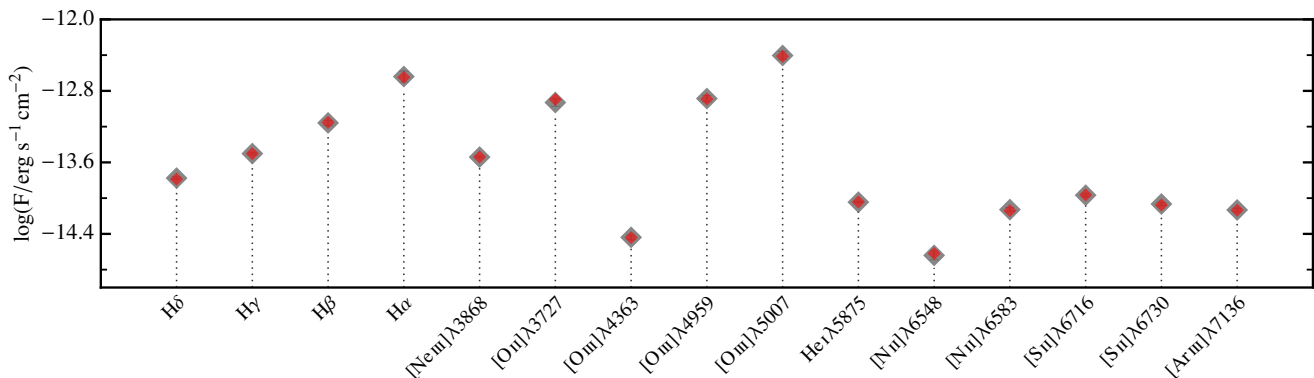


Figure 2. Example of a BEAGLE fitting of the galaxy with SB 80. Data are indicated by grey diamonds, model fluxes by red ones. Both fluxes are uncorrected for internal extinction. Note that the error bars on the data points are contained within the markers.

photoionized gas (Gutkin et al. 2016). We adopt a Chabrier (2003) stellar IMF truncated at 0.1 and $100 M_{\odot}$, constant star formation rate, and take galaxy age t (time since onset of star formation) and metallicity (assumed to be the same for the stars, Z , as for the gas, Z_{ISM}) to be adjustable parameters. We fix the density of the photoionized gas at $n_{\text{H}} = 10^2 \text{ cm}^{-3}$ but allow the ionization parameter $\log U_{\text{S}}$, which sets the ratio of H-ionizing-photon to gas density at the Strömgen radius,² the dust-to-metal mass ratio ξ_{d} , which sets the depletion of heavy elements onto dust grains, and the C/O abundance ratio, to vary. Following S17, we adopt an SMC extinction curve (Pei 1992) to model attenuation by dust in the neutral ISM, as justified by the fact that geometry and scattering effects should have only a minor influence on line emission from the small physical regions probed by our data.

Fig. 2 shows, as an example, the BEAGLE fit of object SB 80, an embedded H II region at $z = 0.01085$ showing WR features in the UV and optical spectra. In Figs 1a,b, we report the line ratios predicted by BEAGLE for all fitted objects in our sample. In general, the agreement between model and data is remarkable, although for about half of the objects, the strengths of [N II] $\lambda 6548$ and [N II] $\lambda 6584$ are slightly underestimated by our model (by ~ 0.15 dex). The emission lines in Fig. 2 are sensitive to dust attenuation (Balmer lines), ionization parameter (e.g. [O III] $\lambda 4959, 5007/\text{H}\beta$), hardness of ionizing radiation (e.g. [O III] $\lambda 4959, 5007/[\text{O II}] \lambda 3726, 3729$), electron temperature ($[\text{O III}] \lambda 4363/[\text{O III}] \lambda 4959, 5007$) and density ($[\text{S II}] \lambda 6731/[\text{S II}] \lambda 6716$), and abundances of O, S, N, Ne and Ar. The simultaneous matching of all these features is therefore a remarkable proof of the validity of our self-consistent physical model.

Table 1 lists the gas-phase O abundances, $\log(\text{O}/\text{H})$, and ionization parameters, $\log U_{\text{S}}$, derived from this analysis. In Fig. 3 we compare $\log(\text{O}/\text{H})$ derived in this way with that obtained by S17 using the ‘direct- T_e ’ method (see their section 3.2). The agreement between both estimates is generally good, although there is some tension in the case of SB 191, the object with highest ionization parameter ($\log U_{\text{S}} \sim -2.1$) in the sample. This may be an indication of the limitation of the ‘direct- T_e ’ method (see also section 5.2 of Gutkin et al. 2016) for such extreme objects, but more data points are necessary to perform a statistical analysis. The ionization parameters in Table 1 are in good overall agreement with those derived by S17 from the analysis of a more limited set of UV-to-optical

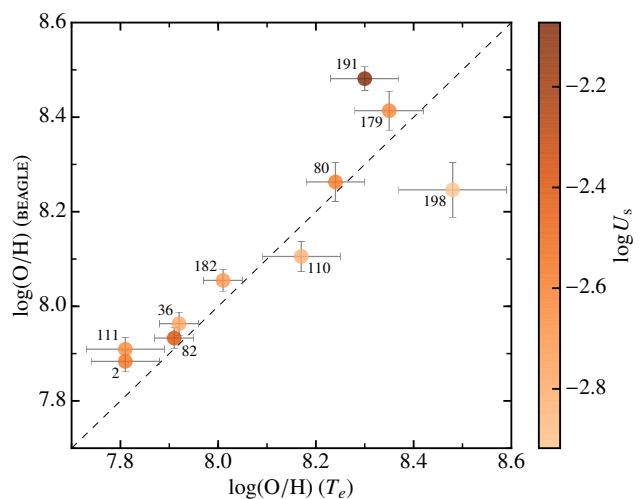


Figure 3. Comparison between the gas-phase metallicity $\log(\text{O}/\text{H})$ obtained in this work with the BEAGLE tool (y-axis) and by S17 with the ‘direct- T_e ’ method. Colour-coded is the ionization parameter $\log U_{\text{S}}$ obtained with the BEAGLE analysis. Error bars indicate the 68 per cent central credible region.

emission lines (see their table 9). The self-consistent modelling of the UV and optical spectra of our objects, including stellar winds features, will be the subject of a follow-up study.

2.2 Production rate of H-ionizing photons

To compute ξ_{ion}^* (Section 1), we must estimate the intrinsic rest-frame UV luminosity L_{UV}^* of the galaxies. We achieve this through a new fit combining SDSS photometry with a UV magnitude obtained from the *HST*/COS spectra³ of S17. Because of different filter configurations used in acquiring the COS data, we use a rectangular filter covering the region $\lambda \sim 1620 - 1660 \text{ \AA}$ to integrate the COS spectra of SB 36 and SB 182, and a filter covering $\lambda \sim 1480 - 1515 \text{ \AA}$ for the other 8 objects. Both regions sample the rest-frame UV continuum of the galaxies, and are not significantly affected by emission lines or ISM absorption lines. We fit the com-

² This parametrization translates into a volume-averaged ionization parameter $\langle U \rangle = 9/4 U_{\text{S}}$ (see equation 1 of Hirschmann et al. 2017).

³ Note that we do not use GALEX photometry, to avoid potential biases introduced by the large GALEX PSF.

ID	$\log(\text{O}/\text{H})$	$\log U_S$	$\log \xi_{\text{ion}}^*$	$\log \xi_{\text{ion}}$
2	7.88 ± 0.02	-2.57 ± 0.02	25.89 ± 0.01	26.47 ± 0.01
36	7.96 ± 0.02	-2.78 ± 0.02	25.19 ± 0.02	25.37 ± 0.03
80	8.26 ± 0.04	-2.60 ± 0.08	25.73 ± 0.02	26.30 ± 0.02
82	7.93 ± 0.02	-2.41 ± 0.02	25.82 ± 0.01	25.81 ± 0.01
110	8.11 ± 0.03	-2.84 ± 0.02	25.20 ± 0.01	25.23 ± 0.01
111	7.91 ± 0.03	-2.67 ± 0.02	25.40 ± 0.03	25.49 ± 0.06
179	8.41 ± 0.04	-2.64 ± 0.04	25.40 ± 0.03	25.92 ± 0.06
182	8.05 ± 0.02	-2.72 ± 0.02	25.61 ± 0.06	25.70 ± 0.11
191	8.48 ± 0.03	-2.07 ± 0.05	26.06 ± 0.02	26.19 ± 0.02
198	8.25 ± 0.06	-2.92 ± 0.05	25.48 ± 0.02	25.65 ± 0.02

Table 1. Gas-phase metallicity $\log(\text{O}/\text{H})$, ionization parameter $\log U_S$, production rate of H-ionizing photons per unit UV ‘intrinsic’ (ξ_{ion}^*) and ‘observed’ (ξ_{ion}) luminosity for the 10 star forming regions analysed in this work. The reported values of each parameter correspond to the posterior median, while the errors indicate to the 68 per cent central credible interval.

bination of SDSS *ugri*⁴ photometry and COS UV magnitude with a model similar to that used to fit the emission line fluxes, but fixing $\text{C}/\text{O} = (\text{C}/\text{O})_{\odot}$ and $\xi_{\text{d}} = 0.3$ to account for the lower constraining power of broad-band data on the gas properties.

We combine the rest-frame intrinsic UV stellar luminosity L_{UV}^* (averaged over a 100 Å-wide rectangular filter centred at $\lambda = 1500$ Å, Robertson et al. 2013) inferred from these fits with the rate of H-ionizing photons \dot{N}_{ion} obtained by fitting the 15 optical emission lines to estimate $\xi_{\text{ion}}^* = \dot{N}_{\text{ion}}/L_{\text{UV}}^*$ for each object in our sample. We report this in Table 1, along with the rate of ionizing photons per unit ‘observed’ UV luminosity, $\xi_{\text{ion}} = \dot{N}_{\text{ion}}/L_{\text{UV}}$, where L_{UV} includes the effect of starlight transmission through the ISM, i.e., of nebular continuum emission and dust attenuation.

In Fig. 4, we plot ξ_{ion}^* against EW of the $[\text{O III}] \lambda\lambda 4959, 5007$ doublet. Objects exhibiting larger $\text{EW}([\text{O III}])$ also show larger ξ_{ion}^* . A relation between the two quantities is expected, and part of the small scatter visible in Fig. 4 can be ascribed to the relatively narrow range of $[\text{O III}] \lambda\lambda 4959, 5007/\text{H}\beta$ probed by our objects (Fig. 1a). Remarkably, the tight relation in Fig. 4 also implies a limited variation of ionized-gas properties in our objects, since the relation between ξ_{ion}^* and $\text{EW}([\text{O III}])$ depends on the shape of the ionizing spectrum (e.g. stellar age and metallicity), ionization parameter (geometry of the photoionized regions), metal abundances and gas density. The colour coding of the circles in Fig. 4 further indicates the EW of $\text{C III} \lambda\lambda 1907, 1909$ measured from the COS spectra. As noted by S17 (their fig. 10), the EWs of $\text{C III} \lambda\lambda 1907, 1909$ and $[\text{O III}] \lambda\lambda 4959, 5007$ are related to each other, the most extreme C III emitters showing largest $[\text{O III}]$ emission. Additional high-quality rest-frame UV spectra are required to calibrate a relation between ξ_{ion}^* and C III , but this relation has the potential to allow indirect constraints on ξ_{ion}^* even for galaxies deep into the EoR.

We fit the relation between ξ_{ion}^* and $\text{EW}([\text{O III}])$ using ‘Orthogonal Distance Regression’, a linear regression method which allows us to account for errors along both the y- and x-axis.⁵ The black

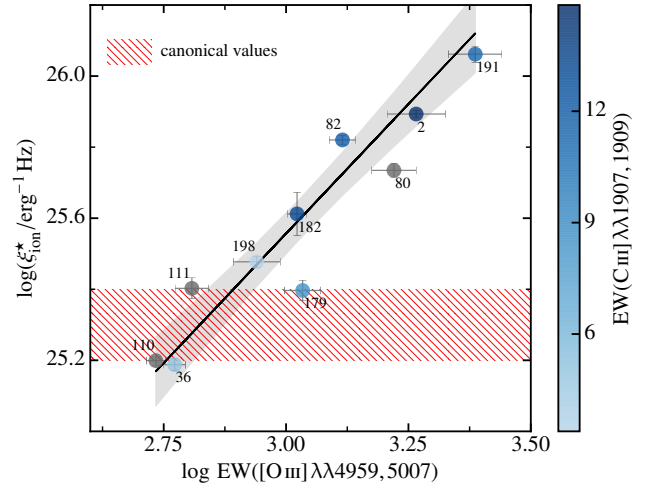


Figure 4. Relation between production rate of H-ionizing photons per unit intrinsic monochromatic UV luminosity (y-axis) and EW of the $[\text{O III}] \lambda\lambda 4959, 5007$ doublet (x-axis). Colour-coded is the equivalent width of $\text{C III} \lambda\lambda 1907, 1909$, while grey circles indicate objects with no $\text{C III} \lambda\lambda 1907, 1909$ detections. Error-bars on the circles indicate the 68 per cent central credible region. The black line indicates the best-fit linear relation between ξ_{ion}^* and $\text{EW}([\text{O III}])$ reported in equation (2.1), while the grey bands indicate the 68 per cent credible region. The red hatched region indicates typical ξ_{ion}^* values adopted in reionization models.

line in Fig. 4 show the best-fitting relation

$$\log \xi_{\text{ion}}^* = 21.18 \pm 0.47 + 1.46 \pm 0.16 \times \log(\text{EW}[\text{O III}]), \quad (2.1)$$

while the grey bands indicate the 68 per cent credible region around the best-fitting relation. We also fit a relation considering the combined EW of $\text{H}\beta + [\text{O III}] \lambda\lambda 4959, 5007$, obtaining a relation with intercept (slope) = 20.99 (1.49) instead of 21.18 (1.46). Such a relation is particularly useful to convert in a physically-motivated way broad-band colour excesses (e.g. IRAC excess, Shim et al. 2011; Stark et al. 2013; Smit et al. 2014) into ξ_{ion}^* values.

2.3 Discussion

The constraints we obtain on ξ_{ion}^* , along with the UV and kinematic properties of our sample, have potentially important implications for our understanding of the sources of H-ionizing photons in pristine star-forming galaxies. The objects in our sample are extremely rare in the nearby Universe, but far more common at high redshift. In the entire SDSS DR7 sample, only ~ 200 galaxies (0.01 per cent) entered our initial selection criteria of $\text{He II} \lambda 4686$ emitters dominated by stellar photoionization. At high redshift, however, the situation appears to be different. Very large EWs of optical emission lines are routinely inferred from contamination of broad-band *Spitzer*/IRAC photometry, corresponding to $\text{EW}(\text{H}\alpha + [\text{N II}] \lambda\lambda 6548, 6584 + [\text{S II}] \lambda\lambda 6716, 6731)$ up to ~ 400 for galaxies at $z \sim 4.5$ (Stark et al. 2013; Smit et al. 2016; Mármol-Queraltó et al. 2016), reaching $\gtrsim 1000$ for galaxies at $z \sim 5.2$ (Rasappu et al. 2016). Smit et al. (2014) derive $\text{EW}(\text{H}\beta + [\text{O III}] \lambda\lambda 4959, 5007) \gtrsim 1000$ for extremely blue IRAC galaxies at $z \sim 7$. Observations of high-ionization UV lines provide a consistent picture: while high EWs of UV lines, such as $\text{C IV} \lambda\lambda 1548, 1551$, $\text{C III} \lambda\lambda 1907, 1909$ and $\text{O III} \lambda\lambda 1660, 1666$, are rare at low redshift, they have been routinely detected at higher redshifts (e.g. Stark et al. 2015a,b, 2017; Mainali et al. 2017). The

⁴ We do not fit the reddest SDSS band (z) since the adopted (constant) star formation histories may introduce biases when fitting a band potentially dominated by evolved stellar populations.

⁵ <https://docs.scipy.org/doc/scipy/reference/odr.html>

emerging picture is that at $z \gtrsim 6$ a combination of high star formation rates per unit stellar mass, young stellar populations, low metallicities and high ionization parameters favour the presence of $EW \gtrsim 1000$ (10) for the brightest optical (UV) lines, which our analysis suggest correspond to values of ξ_{ion}^* significantly larger than canonical values used in reionization models.

From a theoretical perspective, simulations indicate that the escape fraction of H-ionizing photons from galaxies is time-dependent, being tightly coupled to the energy input from stellar feedback (winds, SNe), which opens ‘clear’ channels through which ionizing radiation can escape (e.g. Wise & Cen 2009; Trebitsch et al. 2017). The presence of broad components in the emission lines of our objects suggests that such feedback mechanisms are at work in star-forming regions with a high production efficiency of H-ionizing photons. If regions with high ξ_{ion}^* also exhibit large f_{esc} , then short, powerful bursts of star formation in low-metallicity, low-mass galaxies can provide enough H-ionizing photons to achieve the time-averaged value $\log(f_{\text{esc}} \xi_{\text{ion}}^*/\text{erg}^{-1}\text{Hz}) = 24.5$ (Bouwens et al. 2016) necessary to keep the IGM ionized.⁶

3 CONCLUSIONS

We have analysed a sample of 10 extreme nearby star-forming regions with high-quality UV-to-optical spectra. In the [N II]-BPT diagram, our objects are characterised by low metallicities and high ionization parameters similar to those of the LyC leakers of Izotov et al. (2016). Using a combination of state-of-the-art stellar population+photoionization models incorporated into the BEAGLE spectral analysis tool, we have fitted 15 optical emission lines in these objects, including lines sensitive to dust attenuation, ionizing spectrum, ionization parameter, electrons temperature and density, and metal abundances. The simultaneous matching of this large set of lines is, to our knowledge, one of the most stringent test performed so far on physically coherent models of stars and gas in star-forming regions. The gas-phase O abundances derived through this self-consistent modelling are in good agreement with those obtained with the ‘direct- T_e ’ method.

The rest-frame intrinsic UV luminosities of our objects, L_{UV}^* , estimated from *HST*/COS observations and SDSS photometry, combined with the production rates of H-ionizing photons obtained with the emission-line analysis, \dot{N}_{ion} , yield a range of $\xi_{\text{ion}}^* = \dot{N}_{\text{ion}}/L_{\text{UV}}$ values ($\log \xi_{\text{ion}}^*/\text{erg}^{-1}\text{Hz} \sim 25.2-26.1$), significantly larger than the canonical range typically adopted in reionization models ($\log \xi_{\text{ion}}^*/\text{erg}^{-1}\text{Hz} \sim 25.2-25.4$). Most importantly, we have calibrated a new relation between ξ_{ion}^* and $EW[\text{O III}]\lambda\lambda 4959,5007$ ($EW[\text{O III}]\lambda\lambda 4959,5007 + EW\text{H}\beta$), which can be used to derive ξ_{ion}^* values from existing broad-band observations of galaxies at $z \gtrsim 6$ and future *JWST* spectroscopic observations out to redshift ~ 9.5 .

ACKNOWLEDGEMENTS

JC, SC, and AVG acknowledge support from the European Research Council (ERC) via an Advanced Grant under grant agreement no. 321323-NEOGAL. DPS acknowledges support from the National

Science Foundation through the grant AST-1410155. TJ acknowledges support from NASA through Hubble Fellowship grant HST-HF2-51359.001-A awarded by the Space Telescope Science Institute. AF acknowledges support from the ERC via an Advanced Grant under grant agreement no. 339659-MUSICOS. The data described in this paper were obtained by the MMT Observatory, a joint facility of the University of Arizona and the Smithsonian Institution, and the NASA/ESA Hubble Space Telescope. Support for HST GO program #14168 was provided by NASA through a grant from the Space Telescope Science Institute, which is operated by the Association of Universities for Research in Astronomy, Inc., under NASA contract NAS 5-26555.

References

- Abazajian K. N., et al., 2009, *ApJS*, **182**, 543
 Amorín R., Vílchez J. M., Hägele G. F., Firpo V., Pérez-Montero E., Papaderos P., 2012, *ApJ*, **754**, L22
 Baldwin J. A., Phillips M. M., Terlevich R., 1981, *PASP*, **93**, 5
 Bouwens R. J., et al., 2015, *ApJ*, **803**, 34
 Bouwens R. J., Smit R., Labbé I., Franx M., Caruana J., Oesch P., Stefanon M., Rasappu N., 2016, *ApJ*, **831**, 176
 Bromm V., Yoshida N., 2011, *ARA&A*, **49**, 373
 Bruzual G., Charlot S., 2003, *MNRAS*, **344**, 1000
 Chabrier G., 2003, *PASP*, **115**, 763
 Chevallard J., Charlot S., 2016, *MNRAS*, **462**, 1415
 Fan X., et al., 2006, *AJ*, **132**, 117
 Gutkin J., Charlot S., Bruzual G., 2016, *MNRAS*, **462**, 1757
 Hirschmann M., Charlot S., Feltre A., Naab T., Choi E., Ostriker J. P., Somerville R. S., 2017, preprint, ([arXiv:1706.00010](https://arxiv.org/abs/1706.00010))
 Izotov Y. I., Thuan T. X., Guseva N. G., 2007, *ApJ*, **671**, 1297
 Izotov Y. I., Schaerer D., Thuan T. X., Worseck G., Guseva N. G., Orlová I., Verhamme A., 2016, *MNRAS*, **461**, 3683
 Izotov Y. I., Thuan T. X., Guseva N. G., 2017, *MNRAS*, **471**, 548
 James B. L., Tsamis Y. G., Barlow M. J., Westmoquette M. S., Walsh J. R., Cuisinier F., Exter K. M., 2009, *MNRAS*, **398**, 2
 Mainali R., Kollmeier J. A., Stark D. P., Simcoe R. A., Walth G., Newman A. B., Miller D. R., 2017, *ApJ*, **836**, L14
 Mármod-Queralto E., McLure R. J., Cullen F., Dunlop J. S., Fontana A., McLeod D. J., 2016, *MNRAS*, **460**, 3587
 Mirabel I. F., Dijkstra M., Laurent P., Loeb A., Pritchard J. R., 2011, *A&A*, **528**, A149
 Parsa S., Dunlop J. S., McLure R. J., 2017, preprint, ([arXiv:1704.07750](https://arxiv.org/abs/1704.07750))
 Pei Y. C., 1992, *ApJ*, **395**, 130
 Planck Collaboration et al., 2016, *A&A*, **596**, A108
 Rasappu N., Smit R., Labbé I., Bouwens R. J., Stark D. P., Ellis R. S., Oesch P. A., 2016, *MNRAS*, **461**, 3886
 Robertson B. E., et al., 2013, *ApJ*, **768**, 71
 Schaerer D., Izotov Y. I., Verhamme A., Orlová I., Thuan T. X., Worseck G., Guseva N. G., 2016, *A&A*, **591**, L8
 Schmidt K. B., et al., 2017, *ApJ*, **839**, 17
 Senchyna P., et al., 2017, preprint, ([arXiv:1706.00881](https://arxiv.org/abs/1706.00881))
 Shim H., Chary R.-R., Dickinson M., Lin L., Spinrad H., Stern D., Yan C.-H., 2011, *ApJ*, **738**, 69
 Shirazi M., Brinchmann J., 2012, *MNRAS*, **421**, 1043
 Smit R., et al., 2014, *ApJ*, **784**, 58
 Smit R., Bouwens R. J., Labbé I., Franx M., Wilkins S. M., Oesch P. A., 2016, *ApJ*, **833**, 254
 Smit R., Swinbank A. M., Massey R., Richard J., Smail I., Kneib J.-P., 2017, *MNRAS*, **467**, 3306
 Stark D. P., 2016, *ARA&A*, **54**, 761
 Stark D. P., Schenker M. A., Ellis R., Robertson B., McLure R., Dunlop J., 2013, *ApJ*, **763**, 129
 Stark D. P., et al., 2015a, *MNRAS*, **450**, 1846
 Stark D. P., et al., 2015b, *MNRAS*, **454**, 1393
 Stark D. P., et al., 2017, *MNRAS*, **464**, 469

⁶ This value assumes a minimum UV magnitude $M_{1500} = -13$, while adopting $M_{1500} = -17$ would imply a higher $\log(f_{\text{esc}} \xi_{\text{ion}}^*/\text{erg}^{-1}\text{Hz}) = 24.9$.

- Strom A. L., Steidel C. C., Rudie G. C., Trainor R. F., Pettini M., Reddy N. A., 2017, [ApJ](#), **836**, 164
- Trebitsch M., Blaizot J., Rosdahl J., Devriendt J., Slyz A., 2017, [MNRAS](#), **470**, 224
- Wise J. H., Cen R., 2009, [ApJ](#), **693**, 984
- Wise J. H., Demchenko V. G., Halicek M. T., Norman M. L., Turk M. J., Abel T., Smith B. D., 2014, [MNRAS](#), **442**, 2560

This paper has been typeset from a $\text{\TeX}/\text{\LaTeX}$ file prepared by the author.